Available online at www.sciencedirect.com

ScienceDirect

www.elsevier.com/locate/jes

JES JOURNAL OF ENVIRONMENTAL SCIENCES

www.jesc.ac.cn

Removal of ammonium ion from water by Na-rich birnessite: Performance and mechanisms

Ya Cheng, Tinglin Huang, Xinxin Shi, Gang Wen, Yuankui Sun*

Key Laboratory of Northwest Resource, Environment and Ecology, MOE, Xi'an University of Architecture and Technology, Xi'an 710055, China
Shaanxi Key Laboratory of Environmental Engineering, Xi'an University of Architecture and Technology, Xi'an 710055, China

ARTICLE INFO

Article history:
Received 8 July 2016
Revised 25 November 2016
Accepted 8 December 2016
Available online 29 December 2016

Keywords:
Ammonium ion adsorption
Na-rich birnessite
Hydroxyl ions
Negatively charged surface
Electrostatic interaction

ABSTRACT

Na-rich birnessite (NRB) was synthesized by a simple synthesis method and used as a high-efficiency adsorbent for the removal of ammonium ion (NH_4^+) from aqueous solution. In order to demonstrate the adsorption performance of the synthesized material, the effects of contact time, pH, initial ammonium ion concentration, and temperature were investigated. Adsorption kinetics showed that the adsorption behavior followed the pseudo second-order kinetic model. The equilibrium adsorption data were fitted to Langmuir and Freundlich adsorption models and the model parameters were evaluated. The monolayer adsorption capacity of the adsorbent, as obtained from the Langmuir isotherm, was 22.61 mg NH_4^+-N/g at 283 K. Thermodynamic analyses showed that the adsorption was spontaneous and that it was also a physisorption process. Our data revealed that the higher NH_4^+ adsorption capacity could be primarily attributed to the water absorption process and electrostatic interaction. Particularly, the high surface hydroxyl-content of NRB enables strong interactions with ammonium ion. The results obtained in this study illustrate that the NRB is expected to be an effective and economically viable adsorbent for ammonium ion removal from aqueous system.

Introduction

Ammonium ion (NH_4^+) is the primary nitrogen polluting species in the hydrosphere. Ammonium ion discharged together with municipal, agricultural or industrial effluents is responsible for harmful effects such as eutrophication of lakes and rivers, decreased dissolved oxygen, toxicity to aquatic life, and increased corrosion rate of soil materials (Karadag et al., 2006; Yusof et al., 2010). Eutrophication of water bodies, a problem of global concern, has been identified as a major environmental problem for water resource management (Du et al., 2005; Zheng et al., 2008). In water supply plants, the ammonium ion present in raw water will react with chlorine to form disinfection byproducts, which could damage the human nervous system and cause deterioration of the taste and odor of water. Hence, it is necessary either to control the ammonium ion contamination in raw water or to remove it before the water is disinfected with chlorine (Cai et al., 2015; Han et al., 2013). Controlling the ammonium ion in the raw water is the preferred solution.

A number of methods (*e.g.*, ion-exchange, adsorption) have been developed to remove ammonium ion (Leaković et al., 2000; Liu et al., 2015; Mandowara and Bhattacharya, 2011; McVeigh and Weatherley, 1999; Wang et al., 2014). Among these strategies, adsorption is considered to be promising due to its high-efficiency, cost effectiveness and easy implementation (Zhu et al., 2012). As a result, many natural and synthetic materials have been developed and used as adsorbents for ammonium ion removal. However, these adsorbents were always found to have slow adsorption kinetics, and their adsorption capacities may be limited (Alshameri et al., 2014;

* *Corresponding author*. E-mail: huangtinglin@xauat.edu.cn (Tinglin Huang).

http://dx.doi.org/10.1016/j.jes.2016.11.015
1001-0742/

Kučić et al., 2012; Moradi, 2011; Nielsen, 1996; Rožić et al., 2000). In addition, increased awareness and understanding of the deleterious effects of ammonium ion released from wastewater treatment facilities into natural water systems has resulted in stringent laws restricting ammonium ion discharge. Therefore, the development of new adsorbents designed specifically for the rapid removal of ammonium ion from water is necessary.

Manganese oxides (MnO_x) with layered topologies are ubiquitous in the natural environment. Birnessite belongs to the family of layered hydrous manganese oxides. It possesses unique surface charge, cation exchange, and redox properties, which make it highly reactive with respect to sorption phenomena. Furthermore, birnessite can be synthesized easily under laboratory conditions and, consequently, has often been applied to remove heavy metals (*e.g.*, copper, cadmium, lead and zinc) from water (Eren, 2009; Gadde and Laitinen, 1974; Han et al., 2006a, 2006b; Lefkowitz and Elzinga, 2015; Wang et al., 2007; Kanungo et al., 2004; McKenzie, 1980; Villalobos et al., 2005).

To the best of our knowledge, studies on the adsorption of ammonium ion by manganese oxide in water solution have been limited. Birnessite is the predominant naturally occurring manganese oxide in most environmental settings (Zhu et al., 2010). Thus, in this study, we examined the adsorption of ammonium ion from water by a birnessite-type manganese oxide. The adsorption kinetics and equilibrium isotherms of the uptake of ammonium ion on manganese oxide were studied. Additionally, the effects of initial ammonium ion concentration, contact time, pH, and the major ions present in groundwater on the adsorption process were investigated. The structural characterization of the adsorbents was used to preliminarily reveal the underlying sorption mechanism.

1. Materials and methods

1.1. Materials

Manganese chloride ($MnCl_2{\cdot}4H_2O$), potassium permanganate ($KMnO_4$), sodium hydroxide (NaOH), ammonium chloride (NH_4Cl), calcium chloride ($CaCl_2$), and magnesium chloride ($MgCl_2$) were of analytical reagent grade. All solutions were prepared with deionized distilled water. NH_4^+-N solutions of different concentrations were prepared by dissolving the required amounts of NH_4Cl in deionized distilled water.

1.2. Preparation of absorbent

Birnessite-type manganese oxides with interlayer K^+ and Na^+ ions have been synthesized by redox reactions between $KMnO_4$ and $MnCl_2$ under alkaline conditions. In this study, the absorbent sample was prepared based on the method reported by Luo and Suib (1997). Specifically, 160 mL of 0.5 mol/L $MnCl_2{\cdot}4H_2O$ was added into 180 mL of 5.55 mol/L NaOH under constant stirring. After 2 hr of cooling, 160 mL of 0.2 mol/L $KMnO_4$ was added dropwise under constant stirring. The manganese oxide formed was allowed to settle and the supernatant was replaced with water several times until no more manganese ion was detected in the washing water. The resultant sample was freeze-dried, ground, and sieved through a 100 mesh sieve before being used.

Birnessite is a layered Mn oxide consisting of stacked sheets of edge-sharing MnO_6 octahedra with water molecules in the interlayer space (Elzinga, 2011; Drits et al., 1998; Nakayama et al., 2008). Furthermore, due to the Mn site vacancies and substitution of Mn(III) for Mn(IV), the manganese oxide layer is always negatively charged (Elzinga, 2011), and thus in order to counterbalance the charge defects in MnO_6 sheets, cations (*e.g.*, Na^+) will also be intercalated in the interlayer region.

1.3. Characterization of adsorbent

The manganese oxide sample solids were characterized by attenuated total reflectance Fourier transform infrared (ATR–FT–IR) spectroscopy, powder X-ray diffraction (XRD), scanning electron microscopy (SEM) and nitrogen porosimetry to determine MnO_x mineralogy. Samples were randomly selected for characterization. To resolve the bands of functional groups and determine their frequency, spectral analysis was done for MnO_x sample solids before and after NH_4^+ adsorption using an FT-IR spectrometer (Thermo-Nicolet IS50) in the range of 500–4000 cm^{-1}. The structures of the samples were examined by XRD at room temperature using a Rigaku Ultiman IV diffractometer with Cu Kα radiation (λ = 1.5606 Å) operated at 40 kV and 40 mA, with data collected in the range of 5 to 80° at a scan rate of 5°/min and a step size of 0.02°. Phases were identified using JCPDS files. The surface and pore properties of the adsorbent were studied using nitrogen adsorption experiments using an Autosorb-1 (Quantachrome Instruments) at 77 K. The specific surface area of the adsorbent was calculated using the Brunauer–Emmett–Teller (BET) method. SEM images were taken on a Hitachi S-3400 N scanning electron microscope. The voltage used was 5 kV for the SEM studies. Zeta potential was conducted by a Malvern Instruments Zetasizer Nano ZS 90.

1.4. Batch adsorption experiments

Two different types of sorption experiments were performed: kinetics experiments, with reaction times ranging from 0 to 300 min, and isotherm experiments at 283, 293, 303 and 313 K to establish the maximum ammonium ion sorption after 30 min of equilibration, where the concentrations of NH_4^+-N ranged from 2 to 50 mg/L. For both types of experiments, portions of the adsorbent samples were accurately weighed into 250-mL glass conical flasks to yield a final solid concentration of 0.5 g/L. The final volumes were adjusted to 100 mL with deionized distilled water after appropriate volumes of ammonium ion stock solution were added to yield the pre-selected NH_4^+-N concentrations. The initial concentrations of NH_4^+-N in the kinetics experiments were 2–25 mg/L. The suspensions were shaken at 150 r/min on a water bath shaker at 298 K.

To explain the adsorption behavior of manganese oxide, the effect of pH on the NH_4^+ adsorption capacity of manganese oxide was evaluated. The pH values were adjusted using dilute NaOH or HCl. The initial concentrations of NH_4^+-N and manganese oxide used in these experiments were 10 mg/L and 0.5 g/L, respectively. To study the effect of cations (Na^+, Ca^{2+} and Mg^{2+}) on the adsorption capacity, the initial NH_4^+-N concentration of 15 mg/L and individual cation concentrations in the range of 0–75 mg/L were used.

Samples for ammonium ion analysis were obtained by filtration of the suspension through 0.45 μm polyethersulfone syringe filters. The filtrates obtained were examined by the conventional Nesslerization method to determine the NH_4^+-N concentration in solution. The calibration curve was plotted with absorbance as a function of NH_4^+-N concentration in solution. The amount of adsorbed NH_4^+-N at time t, q_t (mg/g), was calculated using the following Eq. (1):

$$q_t = \left(\frac{c_0 - c_t}{m}\right) \times V \quad (1)$$

where, c_0 (mg/L) is initial concentration of NH_4^+-N, c_t (mg/L) is the concentration of NH_4^+-N at time t, V (L) is volume of solution used, and m (g) is the mass of adsorbent sample. Each experiment was performed in triplicate and standard deviations were calculated. Data points in all figures without error bars represented the mean values of triplicate experimental results.

2. Results and discussion

2.1. Phase structure of adsorbent

XRD was used to identify the phases and crystallinity of the synthesized manganese oxide samples (Iyer et al., 2012). The diffractogram obtained for manganese oxide is shown in Fig. 1. The XRD pattern of our sample is almost identical to that reported by Drits et al. (1997). The narrow characteristic peaks in the XRD pattern of the sample indicate high crystallinity. The prepared manganese oxide was composed primarily of Na-rich birnessite (NRB), as indicated by two peaks at d = 7.144 [001] and 3.572 [002] Å in its XRD pattern (XRD JCPDS file 43-1456), which are characteristic for this mineral phase. The sample shows characteristic [200], [110], [310] and [020] peaks of birnessite, which confirms that it has the one-layer monoclinic structure.

2.2. Kinetics of ammonium ion adsorption on NRB

Adsorption kinetic studies were thoroughly explored at 298 K with initial pH 5.8, since they can provide important information on the adsorption rate and mechanism. Fig. 2a shows that the higher the initial NH_4^+ concentration, the greater the adsorption capacity. According to several studies, the initial concentration could provide the driving force to overcome the mass transfer resistance of NH_4^+ between the aqueous and solid phases (Malkoc and Nuhoglu, 2005). An increase in the initial NH_4^+ concentration increased the mass transfer driving force of the NH_4^+ between the aqueous solution and adsorbent phase, which led to an increase in NH_4^+ uptake (Aksu, 2002; Mashitah et al., 2008). The adsorption process nearly reached equilibrium within the first few minutes, which suggested a fast adsorption process. After that, no remarkable concentration changes occurred. It is assumed here that the adsorption takes place primarily at easily accessible surface sites, requiring no diffusion into micro-pores, and the rapid adsorption rate may be attributed to a hydrophobic interaction between the adsorbent and NH_4^+ (Mashitah et al., 2008; Qin et al., 2007).

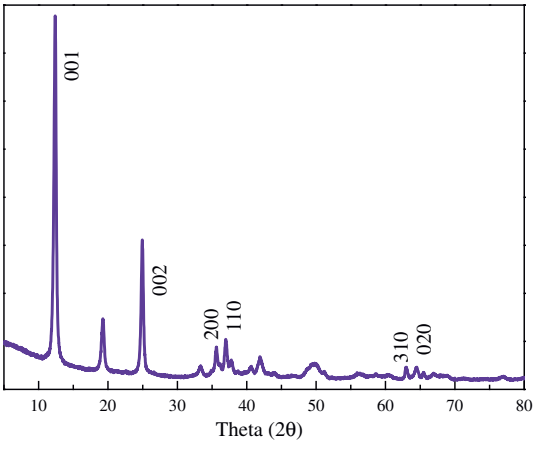

Fig. 1 – X-ray diffractogram of the manganese oxide sample.

Kinetic modeling not only allows estimation of adsorption rates but also enables the determination of suitable rate expressions, characteristic of possible reaction mechanisms. In this respect, the pseudo first-order kinetic model, the pseudo second-order kinetic model and the intra-particle model were used to test the experimental data at the concentration of 10 mg/L NH_4^+-N:

The pseudo first-order model is represented as:

$$\ln q_e - q_t = \ln q_e - k_1 t \quad (2)$$

The pseudo second-order model is represented as:

$$\frac{t}{q_t} = \frac{1}{k_2 q_e^2} + \frac{1}{q_e} t \quad (3)$$

The intra-particle diffusion model is represented by:

$$q_t = k_i t^{1/2} + C \quad (4)$$

where, q_e (mg/g) and q_t (mg/g) represent the amounts of NH_4^+ ion adsorbed at equilibrium and time t (min), respectively. k_1 (min^{-1}) is the rate constant of the pseudo first-order model. k_2 (g/(mg·min)) is the pseudo second-order rate constant. k_i (mg/($min^{1/2}$·g)) is the intra-particle diffusion rate constant and C is the intercept.

The results from fitting experimental data with pseudo first-order, pseudo second-order and intra-particle diffusion models are presented in Table 1. According to the correlation coefficient values, it can be easily determined that the pseudo second-order kinetic model fitted the NH_4^+ adsorption best. The plots of the pseudo second-order kinetic parameters for different NH_4^+-N concentrations are shown in Fig. 2b.

2.3. Adsorption isotherm

In order to optimize the design of an adsorption system, analysis of the adsorption equilibrium data is important. In order to describe the adsorption isotherm, two important isotherms models were selected in this study, *i.e.*, the Langmuir and Freundlich isotherms.

The Langmuir isotherm assumes that the adsorption occurs at specific homogeneous sites on the adsorbent, and is the most commonly used model for monolayer adsorption process, as represented by the following equation (Zheng et al., 2009):

$$q_e = \frac{q_m b C_e}{1 + b C_e} \quad (5)$$

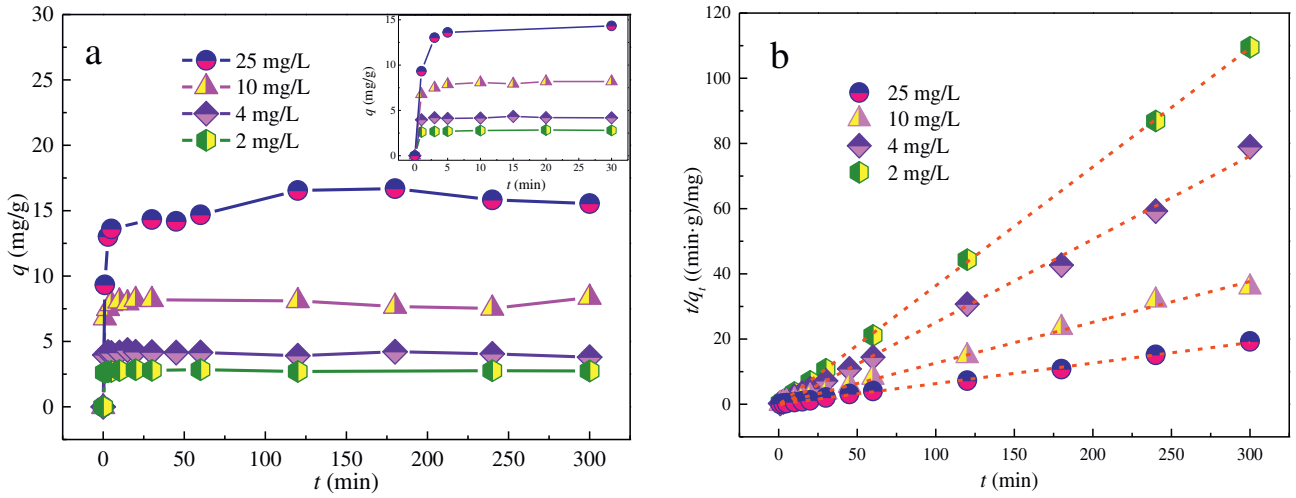

Fig. 2 – Adsorption kinetic (a) and pseudo second-order kinetic model plots (b) for NH_4^+ ion adsorption onto NRB at different initial NH_4^+-N concentrations (2–25 mg/L) (adsorbent dose = 0.5 g/L, pH = 5.8 ± 0.2, shaking speed = 150 r/min, temperature = 298 K). The inset in Fig. 2a shows the same results of adsorption kinetic but has an enlarged scale.

where, q_e (mg/g) is the equilibrium adsorption capacity of NH_4^+-N on adsorbent, C_e (mg/L)s the concentration of NH_4^+-N at equilibrium, q_m (mg/g) is the monolayer adsorption capacity of the adsorbent and b (L/mg) is the Langmuir adsorption constant. These parameters can be determined by non-linear regression of the experimental data.

The Freundlich isotherm equation, the most important multilayer adsorption isotherm for heterogeneous surfaces, is described by the following equation (Öztürk and Bektaş, 2004):

$$\log q_e = \log K_f + \frac{1}{n}\log C_e \quad (6)$$

where, K_f (mg/g)(l/mg)$^{1/n}$ and n are Freundlich adsorption isotherm constants, affecting the adsorption capacity and intensity of adsorption.

Fig. 3 shows the Langmuir and Freundlich plots for the NH_4^+ adsorption at different temperatures. It was clear that adsorption isotherms at different temperatures could be fitted well using the two isotherm models. The isotherm parameters obtained from the fitting curves to the Langmuir and Freundlich models are given in Table 2. However, the Langmuir model was more suitable than the Freundlich model to describe the adsorption isotherm, as reflected by the correlation coefficients (R^2). The results suggested that the adsorbent was homogeneous, and the adsorption film had monolayer coverage. On the other hand, the maximum monolayer adsorption capacity, Q_0, defined as the total capacity of manganese oxide for NH_4^+ adsorption, decreases with increasing temperature, which indicates that a decrease in temperature is favorable for NH_4^+ adsorption. Its maximum value was determined to be 22.61 mg/g at 283 K.

The thermodynamic parameters of the adsorption process, including the changes in the standard free energy (ΔG^0), enthalpy (ΔH^0) and entropy (ΔS^0), were estimated using Eqs. (7) and (8), respectively. The calculated values of the thermodynamic parameters are tabulated in Table 3.

$$\Delta G^0 = -RT\ln K_L \quad (7)$$

$$\ln K_L = \frac{\Delta S^0}{R} - \frac{\Delta H^0}{RT} \quad (8)$$

where, R (J/(mol·K)) is the universal gas law constant; T (K) is the absolute temperature of solution and K_L (L/mol) is the Langmuir constant.

It is noted that the ΔG^0 values are all negative, which indicates that adsorption of NH_4^+ onto manganese oxide is feasible and spontaneous. As expected, it was found that the negative values of ΔG^0 increased with increasing temperature from 283 to 313 K, which indicated that adsorption became more spontaneous. It should be specified that the calculated ΔG^0 value at 313 K (−18.91 kJ/mol) was very close to that of 303 K (−19.05 kJ/mol), which may imply that the temperature effects over the test range (303–313 K) became less significant. The ΔH^0 value is negative for adsorption, indicating that the overall process is exothermic. The positive values of ΔS^0 suggest that the randomness at the solid/solution interface increases with the adsorption process.

Table 1 – Kinetic models for ammonium ion adsorption on Na-rich birnessite (NRB) at 298 K.

Models	Parameters	R^2
Pseudo first-order	$Q_{e,cal}$ = 1.709 mg/g k_1 = 0.0423 min^{-1}	0.56
Pseudo second-order	$Q_{e,cal}$ = 8.252 mg/g k_2 = 0.4298 g/(min·mg)	0.99
Intra-particle diffusion	$Q_{e,cal}$ = 6.790 mg/g k_i = 0.3401 mg/(min$^{1/2}$·g)	0.69

2.4. Effect of pH on ammonium ion adsorption

The adsorption of NH_4^+ onto NRB was studied as a function of pH, as shown in Fig. 4a. The results indicated that adsorption

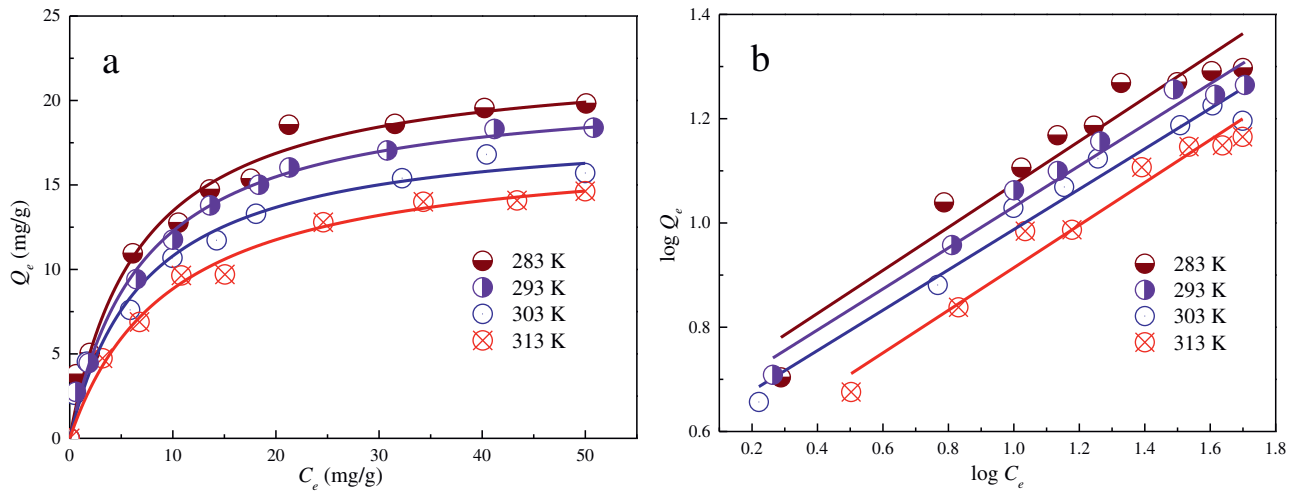

Fig. 3 – Langmuir (a) and Freundlich (b) isotherm equation for NH_4^+ adsorption onto the NRB at different temperatures (initial NH_4^+-N concentrations = 2–50 mg/L, adsorbent dose = 0.5 g/L, pH = 5.8 ± 0.2, shaking speed = 150 r/min). Solid lines represent fitting the data to the Langmuir equation and the Freundlich equation.

capacity of NH_4^+ increased with increasing pH from 2.0 to 5.0, while remaining approximately constant in the pH range of 5.0 to 7.0, then decreased at pH 8.0.

The reason for the poor removal of NH_4^+ at lower pH was that the negative charge on the surface declined due to the excess protons in the solution. This could be demonstrated by the zeta potentials (Fig. 4b). The H^+ ion concentration also increased with the decrease of pH, which intensified its competition for adsorption sites (Huang et al., 2010). The surface charge as assessed by point of zero charge is approximately 2.0, which is consistent with other research results (Kanungo and Parida, 1984; Taffarel and Rubio, 2010). The zeta potential of manganese oxide decreased with the increase of pH, indicating a more negative charge on the manganese oxide surface. The negatively charged surfaces of the manganese oxide can provide the driving force for electrostatic interaction with NH_4^+. This further validates the results obtained in the FT–IR analysis.

After the pH increases to 8.0, the removal efficiency drops dramatically. This behavior can be explained by the fact that NH_4^+ could be converted into NH_3 species at pH values above 8.0 (Du et al., 2005).

Additionally, the equilibrium pH values were shown to increase with an increase in the initial pH from 2.0 to 7.0, and slightly decreased with an additional increase from pH 7.0 to pH 12.0 for all the cases (Fig. 4a); similar results have been reported previously (Wang et al., 2014; Zheng and Wang, 2009).

Table 2 – Parameters of adsorption isotherm of NH_4^+ ion onto manganese oxide at different temperatures.

T(K)	Langmuir			Freundlich		
	Q_0(mg/g)	K_L(L/mg)	R^2	K_F ((mg/g)(L/mg)$^{1/2}$)	1/n	R^2
283	22.61	0.147	0.982	3.169	0.505	0.904
293	20.94	0.142	0.992	3.374	0.469	0.961
303	18.65	0.137	0.980	3.570	0.424	0.970
313	17.5	0.102	0.991	4.261	0.381	0.985

2.5. *Adsorption mechanism*

SEM micrographs (Fig. 5) illustrated the surface morphology of the manganese oxide sample before adsorption. It was apparent that the sample was porous and non-homogeneous. These observations help explain why the adsorbent exhibited an extremely fast rate of adsorption.

FT–IR spectroscopy was used as a direct way of investigating the mechanisms of NH_4^+ adsorption on NRB. The FT–IR spectra of NRB samples collected before and afterthe adsorption of the NH_4^+ from aqueous solution were studied, as shown in Fig. 6. It was reported that the N–H deformation vibration of NH_4Cl occurs at 1415 cm^{-1} (Wang et al., 2014). The main absorption peaks of the NRB can still be observed on the spectra after adsorption. The stretching vibration of hydroxyl ions in specific crystallographic sites was shifted from 3365.5 to 3165.4 cm^{-1}, and the stretching vibration of less-ordered H_2O molecules was shifted from 1644 to 1633 cm^{-1} (Daud and Hameed, 2010; Naidja et al., 2002; Wang et al., 2015). The characteristic adsorption peak of NH_4Cl appeared in the spectra of NRB after adsorption. This information implies that after the adsorption, the surrounding environment of hydroxyl ions and less-ordered H_2O molecules had changed. The results obtained from FT–IR analysis showed that the higher adsorption capacity of NH_4^+ could be mainly attributed to the water absorption process and the electrostatic interaction between NH_4^+ in aqueous solution and –OH groups on NRB. The fast adsorption process nearly reached equilibrium within the first few minutes, which implied a strong electrostatic interaction between the negatively charged surface of manganese oxide and the cationic NH_4^+.

Table 3 – Thermodynamic parameters for NH_4^+ adsorption onto manganese oxide.

T (K)	$\triangle G^0$ (kJ/mol)	$\triangle H^0$ (kJ/mol)	$\triangle S^0$ (J/k mol)
283	−17.95	−8.12	35.19
293	−18.50		
303	−19.05		
313	−18.91		

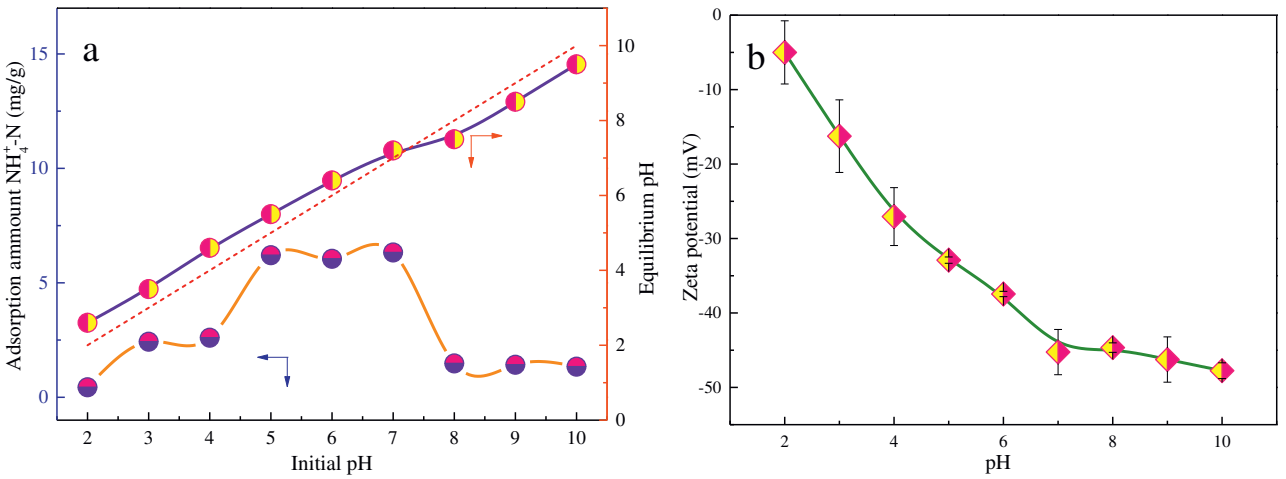

Fig. 4 – Effect of solution pH on the adsorption of NH_4^+ ion onto manganese oxide (a) (initial NH_4^+-N concentration = 10 mg/L, adsorbent dosage = 0.5 g/L, temperature = 298 K); Zeta potential of manganese oxide as a function of pH (b).

It has been reported that the specific surface area is an important factor for determining the adsorption capability of an adsorbent (Auta and Hameed, 2012; Li et al., 2013). The surface area of NRB, as calculated by the standard BET method, is 37 m^2/g. The external surface area and maximum adsorption capacity of NRB and some commonly used adsorbents are listed in Table 4. These are all important and practical adsorbents due to their low-cost, availability and easy application in the removal of ammonium contaminants from the environment. Although the specific surface area is considered to be an important factor for adsorption processes, it can be observed in the table that the maximum adsorption capacity is not positively related to the external surface area. Moreover, it should be noted that the specific surface area of most adsorbents listed in Table 4 is not very high. This phenomenon indicated that the maximum adsorption capacity of an adsorbent for the NH_4^+ is not solely dependent on its specific surface area, and many other factors such as surface morphology and surface charge may also influence the adsorption process. Specifically, the porous and non-homogeneous nature of NRB (as demonstrated in Fig. 5) could also benefit the contact between NRB and the NH_4^+ and thus make the absorption of NH_4^+ more efficient.

On the other hand, the negatively charged surface of manganese oxides, as confirmed by zeta potential, was also favorable for adsorption of positively charged NH_4^+. The point of zero charge (pH_{pzc}) of the manganese oxide is 2–3. Consequently, the manganese oxides are negatively charged at near-neutral pH values. Therefore, because of their specific surface properties, there is an attractive force between NH_4^+ and manganese oxide. NH_4^+ was strongly adsorbed onto the manganese oxide surface. The birnessite group minerals possess low pH_{pzc}, which endows them with significant surface reactivity (Matocha et al., 2001).

The electrostatic attraction can be further verified by performing the adsorption experiment in a mixed solution containing positively charged NH_4^+ and Ca^{2+}, Mg^{2+} and Na^+ cations. It was found that the cations (Ca^{2+}, Mg^{2+} and Na^+) significantly reduce the adsorption of NH_4^+ on manganese oxides. The experimental results obtained for NH_4^+ removal by NRB in the presence of individual cation are shown in Fig. 7. The removal efficiency of the NH_4^+ ion decreased with an increase in the concentration of cations. To further investigate, zeta potential measurements were performed. Without cations the Zeta potential of NRB was –25.0 mV, while in the presence of Ca^{2+}, Na^+ and Mg^{2+}, the Zeta potential of NRB decreased to –15.6 mV, –19.5 mV, and –11.5 mV, respectively.

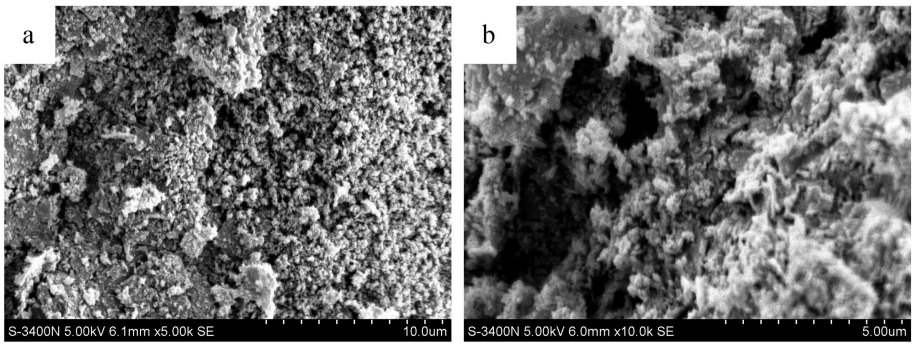

Fig. 5 – Scanning electron microscopy images of the NRB sample at (a) 5000×; (b) 10,000× resolutions.

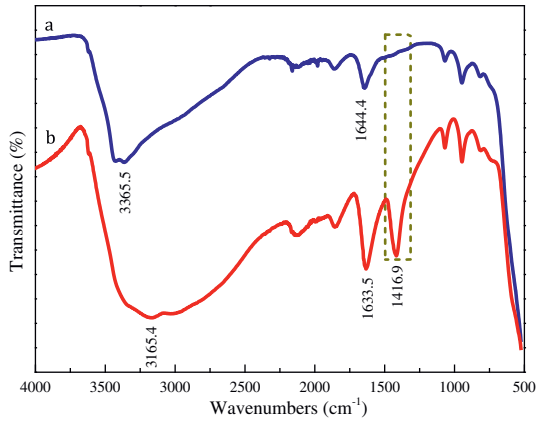

Fig. 6 – Fourier transform infrared spectra of the NRB before (line a) and after (line b) the adsorption of NH_4^+ ion from aqueous solution.

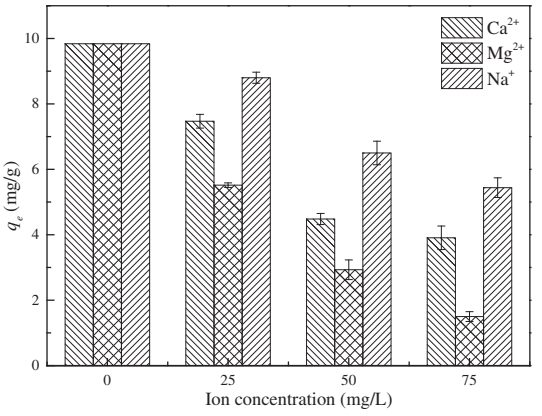

Fig. 7 – Effects of cations (Ca^{2+}, Mg^{2+}, Na^+) on the removal of the NH_4^+ ion (initial NH_4^+-N concentration = 15 mg/L, adsorbent dose = 0.5 g/L, temperature = 298 K).

This effect may be attributed to the preferential absorption of cations and the weakened electronegativity on the NRB surface. It may also be attributed to the competitive adsorption between the cations and NH_4^+.

From the above analysis, it is evident that electrostatic interaction was the main mechanism for the NH_4^+ adsorption. The adsorption process can be described by the following reaction:

$$-NH_4^+ + NRB^- \rightarrow -NH_4^+ \cdot NRB^- \quad (9)$$

where, $-NH_4^+$ represents the NH_4^+ and NRB^- represents a negative site. These aspects mentioned above synergistically contribute to the high adsorption capacity and removal efficiency for NH_4^+.

3. Conclusions

Na-rich birnessite (NRB) has been successfully synthesized by a simple synthesis method. The adsorption ability of NRB was evaluated by choosing the NH_4^+ as a model contaminant. Batch adsorption tests demonstrated that the adsorption is affected by various conditions, such as contact time, solution pH, initial NH_4^+ concentration, and the presence of cations (Ca^{2+}, Mg^{2+} and Na^+). Kinetics data showed that NRB was highly effective for NH_4^+ removal and that the adsorption rate was very high, especially at early stages of the adsorption. Equilibrium data was fitted by the Langmuir and Freundlich isotherms, and was better described by the Langmuir isotherm model, with a maximum monolayer adsorption capacity of 22.61 mg/g. The maximum removal for NH_4^+ was observed at pH 5–7 for NRB. The electrostatic attraction between NRB and NH_4^+ accounts for the high adsorption performance of the NRB. The structure and surface properties of NRB are the key factors affecting its adsorption capacity for NH_4^+. Consequently, these oxides have potential for application in the environmental remediation of NH_4^+.

Acknowledgments

This research was supported by the National Natural Science Foundation of China (No. 51278409) and the Education Department of Shaanxi Province (No.15JS046).

Table 4 – A summary of external surface area and maximum adsorption capacity of some commonly used adsorbents for ammonium ion removal.

Adsorbent	Surface area (m^2/g)	Q_{max} (mg/g)	References
Natural zeolite	2 ± 1	0.38	(Demir et al., 2002)
Yemeni natural zeolite	36	11.0	(Alshameri et al., 2014)
Zeolite clinoptilolite	26	12.29	(Vassileva and Voikova, 2009)
Zeolite synthesized from fly ash	27	24.3	(Zhang et al., 2011a)
Low-calcium fly ashes	27	23.8	(Zhang et al., 2011b)
Low-cost Romanian volcanic tuff	52	19.0	(Maranon et al., 2006)
limestone and rice husk carbon	61	32.89	(Halim et al., 2010)
Sepiolite	263	49	(Balci and Dinçel, 2002)
NRB	37	22.61	This paper

NRB: Na-rich birnessite.

REFERENCES

Aksu, Z., 2002. Determination of the equilibrium, kinetic and thermodynamic parameters of the batch biosorption of nickel (II) ions onto *Chlorella vulgaris*. Process Biochem. 38 (1), 89–99.

Alshameri, A., Ibrahim, A., Assabri, A.M., Lei, X., Wang, H., Yan, C., 2014. The investigation into the ammonium removal performance of Yemeni natural zeolite: modification, ion exchange mechanism, and thermodynamics. Powder Technol. 258, 20–31.

Auta, M., Hameed, B., 2012. Modified mesoporous clay adsorbent for adsorption isotherm and kinetics of methylene blue. Chem. Eng. J. 198, 219–227.

Balci, S., Dinçel, Y., 2002. Ammonium ion adsorption with sepiolite: use of transient uptake method. Chem. Eng. Process. 41 (1), 79–85.

Cai, Y.A., Li, D., Liang, Y., Luo, Y., Zeng, H., Zhang, J., 2015. Effective start-up biofiltration method for Fe, Mn, and ammonium ion removal and bacterial community analysis. Bioresour. Technol. 176, 149–155.

Daud, N., Hameed, B., 2010. Decolorization of Acid Red 1 by Fenton-like process using rice husk ash-based catalyst. J. Hazard. Mater. 176 (1), 938–944.

Demir, A., Gunay, A., Debik, E., 2002. Ammonium removal from aqueous solution by ion-exchange using packed bed natural zeolite. Water SA 28 (3), 329–336.

Drits, V.A., Silvester, E., Gorshkov, A.I., Manceau, A., 1997. Structure of synthetic monoclinic Na-rich birnessite and hexagonal birnessite: I. Results from X-ray diffraction and selected-area electron diffraction. Am. Mineral. 82 (9), 946–961.

Drits, V.A., Lanson, B., Gorshkov, A.I., Manceau, A., 1998. Substructure and superstructure of four-layer Ca-exchanged birnessite. Am. Mineral. 83 (1), 97–118.

Du, Q., Liu, S., Cao, Z., Wang, Y., 2005. Ammonium ion removal from aqueous solution using natural Chinese clinoptilolite. Sep. Purif. Technol. 44 (3), 229–234.

Elzinga, E.J., 2011. Reductive transformation of birnessite by aqueous Mn (II). Environ. Sci. Technol. 45 (15), 6366–6372.

Eren, E., 2009. Removal of lead ions by Unye (Turkey) bentonite in iron and magnesium oxide-coated forms. J. Hazard. Mater. 165 (1), 63–70.

Gadde, R.R., Laitinen, H.A., 1974. Heavy metal adsorption by hydrous iron and manganese oxides. Anal. Chem. 46 (13), 2022–2026.

Halim, A.A., Aziz, H.A., Johari, M.A.M., Ariffin, K.S., 2010. Comparison study of ammonia and COD adsorption on zeolite, activated carbon and composite materials in landfill leachate treatment. Desalination 262, 31–35.

Han, R., Zou, W., Li, H., Li, Y., Shi, J., 2006a. Copper (II) and lead (II) removal from aqueous solution in fixed-bed columns by manganese oxide coated zeolite. J. Hazard. Mater. 137 (2), 934–942.

Han, R., Zou, W., Zhang, Z., Shi, J., Yang, J., 2006b. Removal of copper (II) and lead (II) from aqueous solution by manganese oxide coated sand: I. Characterization and kinetic study. J. Hazard. Mater. 137 (1), 384–395.

Han, M., Zhao, Z.W., Gao, W., Cui, F.Y., 2013. Study on the factors affecting simultaneous removal of ammonium ion and manganese by pilot-scale biological aerated filter (BAF) for drinking water pre-treatment. Bioresour. Technol. 145, 17–24.

Huang, H., Xiao, X., Yan, B., Yang, L., 2010. Ammonium removal from aqueous solutions by using natural Chinese (Chende) zeolite as adsorbent. J. Hazard. Mater. 175 (1), 247–252.

Iyer, A., Delpilar, J., King'Ondu, C.K., Kissel, E., Garces, H.F., Huang, H., ElSawy, A.M., Dutta, P.K., Suib, S.L., 2012. Water oxidation catalysis using amorphous manganese oxides, octahedral molecular sieves (oms-2), and octahedral layered (ol-1) manganese oxide structures. J. Phys. Chem. C 116 (10), 6474–6483.

Kanungo, S., Parida, K., 1984. Interfacial behavior of some synthetic MnO_2 samples during their adsorption of Cu^{2+} and Ba^{2+} from aqueous solution at 300 K. J. Colloid Interface Sci. 98 (1), 252–260.

Kanungo, S.B., Tripathy, S.S., Mishra, S.K., Sahoo, B., 2004. Adsorption of Co^{2+}, Ni^{2+}, Cu^{2+}, and Zn^{2+} onto amorphous hydrous manganese dioxide from simple (1–1) electrolyte solutions. J. Colloid Interface Sci. 269 (1), 11–21.

Karadag, D., Koc, Y., Turan, M., Armagan, B., 2006. Removal of ammonium ion from aqueous solution using natural Turkish clinoptilolite. J. Hazard. Mater. 136 (3), 604–609.

Kučić, D., Markić, M., Briški, F., 2012. Ammonium adsorption on natural zeolite (clinoptilolite): adsorption isotherms and kinetics modeling. Holist. Approach Environ. 2 (4), 145–158.

Leaković, S., Mijatović, I., Cerjan-Stefanović, Š., Hodžić, E., 2000. Nitrogen removal from fertilizer wastewater by ion exchange. Water Res. 34 (1), 185–190.

Lefkowitz, J.P., Elzinga, E.J., 2015. Impacts of aqueous Mn (II) on the sorption of Zn (II) by hexagonal birnessite. Environ. Sci. Technol. 49 (8), 4886–4893.

Li, Y., Du, Q., Liu, T., Peng, X., Wang, J., Sun, J., Wang, Y., Wu, S., Wang, Z., Xia, Y., 2013. Comparative study of methylene blue dye adsorption onto activated carbon, graphene oxide, and carbon nanotubes. Chem. Eng. Res. Des. 91 (2), 361–368.

Liu, B., Giannis, A., Zhang, J., Chang, V.W.C., Wang, J.Y., 2015. Air stripping process for ammonium ion recovery from source-separated urine: modeling and optimization. J. Chem. Technol. Biotechnol. 90 (12), 2208–2217.

Luo, J., Suib, S.L., 1997. Preparative parameters, magnesium effects, and anion effects in the crystallization of birnessites. J. Phys. Chem. C 101 (49), 10403–10413.

Malkoc, E., Nuhoglu, Y., 2005. Investigations of nickel (II) removal from aqueous solutions using tea factory waste. J. Hazard. Mater. 127 (1), 120–128.

Mandowara, A., Bhattacharya, P.K., 2011. Simulation studies of ammonium ion removal from water in a membrane contactor under liquid–liquid extraction mode. J. Environ. Manag. 92 (1), 121–130.

Maranon, E., Ulmanu, M., Fernandez, Y., Anger, I., Castrillón, L., 2006. Removal of ammonium from aqueous solutions with volcanic tuff. J. Hazard. Mater. 137 (3), 1402–1409.

Mashitah, M., Azila, Y.Y., Bhatia, S., 2008. Biosorption of cadmium (II) ions by immobilized cells of *Pycnoporus sanguineus* from aqueous solution. Bioresour. Technol. 99 (11), 4742–4748.

Matocha, C.J., Elzinga, E.J., Sparks, D.L., 2001. Reactivity of Pb (II) at the Mn (III, IV)(oxyhydr) oxide-water interface. Environ. Sci. Technol. 35 (14), 2967–2972.

McKenzie, R., 1980. The adsorption of lead and other heavy metals on oxides of manganese and iron. Soil Res. 18 (1), 61–73.

McVeigh, R., Weatherley, L., 1999. Ammonium ion (NH_4^+) removal from secondary effluent through ion-exchange: the effect of biological activity and the presence of other cations. Water Sci. Technol. 40 (2), 143–149.

Moradi, O., 2011. Applicability comparison of different models for ammonium ion adsorption by multi-walled carbon nanotube. Arab. J. Chem. http://dx.doi.org/10.1016/j.arabjc.2011.12.014.

Naidja, A., Liu, C., Huang, P., 2002. Formation of protein–birnessite complex: XRD, FTIR, and AFM analysis. J. Colloid Interface Sci. 251 (1), 46–56.

Nakayama, M., Kanaya, T., Lee, J.W., Popov, B.N., 2008. Electrochemical synthesis of birnessite-type layered manganese oxides for rechargeable lithium batteries. J. Power Sources 179 (1), 361–366.

Nielsen, P.H., 1996. Adsorption of ammonium to activated sludge. Water Res. 30 (3), 762–764.

Öztürk, N., Bektaş, T.E., 2004. Nitrate removal from aqueous solution by adsorption onto various materials. J. Hazard. Mater. 112 (1), 155–162.

Qin, Q., Ma, J., Liu, K., 2007. Adsorption of nitrobenzene from aqueous solution by MCM-41. J. Colloid Interface Sci. 315 (1), 80–86.

Rožić, M., Cerjan-Stefanović, Š., Kurajica, S., Vančina, V., Hodžić, E., 2000. Ammonium ioncal nitrogen removal from water by treatment with clays and zeolites. Water Res. 34 (14), 3675–3681.

Taffarel, S.R., Rubio, J., 2010. Removal of Mn^{2+} from aqueous solution by manganese oxide coated zeolite. Miner. Eng. 23 (14), 1131–1138.

Vassileva, P., Voikova, D., 2009. Investigation on natural and pretreated Bulgarian clinoptilolite for ammonium ions removal from aqueous solutions. J. Hazard. Mater. 170 (2), 948–953.

Villalobos, M., Bargar, J., Sposito, G., 2005. Mechanisms of Pb (II) sorption on a biogenic manganese oxide. Environ. Sci. Technol. 39 (2), 569–576.

Wang, S.G., Gong, W.X., Liu, X.W., Yao, Y.W., Gao, B.Y., Yue, Q.Y., 2007. Removal of lead (II) from aqueous solution by adsorption onto manganese oxide-coated carbon nanotubes. Sep. Purif. Technol. 58 (1), 17–23.

Wang, X., Lü, S., Gao, C., Xu, X., Zhang, X., Bai, X., Liu, M., Wu, L., 2014. Highly efficient adsorption of ammonium onto palygorskite nanocomposite and evaluation of its recovery as a multifunctional slow-release fertilizer. Chem. Eng. J. 252, 404–414.

Wang, H., Sun, Y., Zhu, T., Wang, W., Deng, H., 2015. Adsorption of acetaldehyde onto carbide-derived carbon modified by oxidation. Chem. Eng. J. 273, 580–587.

Yusof, A.M., Keat, L.K., Ibrahim, Z., Majid, Z.A., Nizam, N.A., 2010. Kinetic and equilibrium studies of the removal of ammonium ions from aqueous solution by rice husk ash-synthesized zeolite Y and powdered and granulated forms of mordenite. J. Hazard. Mater. 174 (1), 380–385.

Zhang, M., Zhang, H., Xu, D., Han, L., Niu, D., Tian, B., Zhang, J., Zhang, L.Y., Wu, W., 2011a. Removal of ammonium from aqueous solutions using zeolite synthesized from fly ash by a fusion method. Desalination 271 (1), 111–121.

Zhang, M., Zhang, H., Xu, D., Han, L., Niu, D., Zhang, J., Zhang, L.Y., Wu, W., 2011b. Ammonium removal from aqueous solution by zeolites synthesized from low-calcium and high-calcium fly ashes. Desalination 277 (1), 46–53.

Zheng, Y., Wang, A., 2009. Evaluation of ammonium removal using a chitosan-g-poly (acrylic acid)/rectorite hydrogel composite. J. Hazard. Mater. 171 (1), 671–677.

Zheng, H., Han, L., Ma, H., Zheng, Y., Zhang, H., Liu, D., Liang, S., 2008. Adsorption characteristics of ammonium ion by zeolite 13X. J. Hazard. Mater. 158 (2), 577–584.

Zheng, Y., Zhang, J., Wang, A., 2009. Fast removal of ammonium nitrogen from aqueous solution using chitosan-g-poly (acrylic acid)/attapulgite composite. Chem. Eng. J. 155 (1), 215–222.

Zhu, M., Ginder-Vogel, M., Sparks, D.L., 2010. Ni (II) sorption on biogenic Mn-oxides with varying Mn octahedral layer structure. Environ. Sci. Technol. 44 (12), 4472–4478.

Zhu, K., Fu, H., Zhang, J., Lv, X., Tang, J., Xu, X., 2012. Studies on removal of NH_4^+-N from aqueous solution by using the activated carbons derived from rice husk. Biomass Bioenergy 43, 18–25.